Journal of Crystal Growth, Volume 475, October 2017, pp. 192-201
DOI:10.1016/j.jcrysgro.2017.05.029

The Growth and Perfection of β-Cyclotetramethylene-tetranitramine (HMX) Studied by Laboratory and Synchrotron X-Ray Topography

H.G. Gallagher[1], J.N. Sherwood[1*] and R.M Vrcelj[2]

[1] WESTChem, Department of Pure and Applied Chemistry, Thomas Graham Building, University of Strathclyde, G1 1XL.

[2]Centre for Defence Chemistry, Cranfield University, Defence Academy of the UK, Shrivenham, SN6 8LA

Corresponding Author: Email: j.n.sherwood@strath.ac.uk

Abstract

An examination has been made of the defect structure of crystals of the energetic material β-cyclotetramethylene-tetranitramine (HMX) using both Laboratory (Lang method) and Synchrotron (Bragg Reflection and Laue method) techniques. The results of the three methods are compared with particular attention to the influence of potential radiation damage caused to the samples by the latter, more energetic, technique. The comparison shows that both techniques can be confidently used to evaluate the defect structures yielding closely similar results. The results show that, even under the relatively casual preparative methods used (slow evaporation of unstirred solutions at constant temperature), HMX crystals of high perfection can be produced. The crystals show well defined bulk defect structures characteristic of organic materials in general: growth dislocations, twins, growth sector boundaries, growth banding and solvent inclusions. The distribution of the defects in specific samples is correlated with the morphological variation of the grown crystals. The results show promise for the further evaluation and characterisation of the structure and properties of dislocations and other defects and their involvement in mechanical and energetic processes in this material.

Keywords: A1 Crystal Morphology; A1 Defects; A1 X-Ray Topography; A2 Growth From Solutions; B1 Organic Compounds

1 Introduction

The mechanical and crystal growth properties of materials are dependent upon not only their atomic structure, but also on the defects that the crystalline form contains. Whilst this is very well understood for simple materials such as metals, for more complex solids such as organic phases, the correlation between defect structure and mechanical properties is less well defined.

Establishing the defect structure of organic materials can be problematic as they have a more complex molecular packing and generally lower symmetry than other materials. This will inevitably result in different dislocation behavior to other crystalline forms. Although methods such as electron microscopy and etching studies can give information regarding defects emergent at organic crystal surfaces, a more complete picture of dislocation and defect distribution can only be obtained by using X-ray diffraction topography. [1]

In addition to the mechanical and crystal growth properties, monitoring defects and dislocations within crystals is an important part of understanding their subsequent downstream usage. Such studies are proving to be of great interest to a wide range of scientific communities studying organic semi-conductors, proteins, non-linear optoelectronics and energetic materials. [2-7]

Historically, it had been thought that dislocation “pile-ups” in energetic materials could generate “hot-spots” which would contribute to premature

ignition, but a pure dislocation "pile-up" mechanism only leads to sub-critical hot spots. [8] The nature of internal defects is still important however, especially when attempting to understand ignition processes at elevated temperatures. [9-11]. At these temperatures, the breakdown in mechanical properties and changes within crystalline particulates can affect localised ongoing heating and decomposition processes. Thus knowledge of the defect structure is essential to understanding later heat driven phenomena.

The importance of elasticity in crystalline energetic materials has also been recognised and is the subject of a recent review [12]. As a consequence, a wide range of materials have been studied both experimentally and theoretically. There is however a lack of detailed knowledge of the nature and influence of inevitably included lattice imperfections on these properties. [13,14]

The internal defect structure of a number of energetic materials has been studied (TNT, RDX and PETN [5,6,15-18]. To add to this range of commonly used energetic materials, we have studied the dislocation and defect distribution of β-cyclotetramethylene-tetranitramine (HMX, $C_4H_8N_8O_8$).

HMX exists in a number of pure polymorphic conformational states, α, β, δ and ε [19-25]. It is also found as a hydrated form, γ [26]. The most stable of the forms at room temperature is the β form, with a unit cell of a = 0.6525nm, b =

1.1037nm, c = 0.7364nm, beta = 102.66°, SG = $P2_1/n$ (after Eiland and Pepinsky and Cady et al [19,20]).

Previously, a dislocation etching technique [27] was used to investigate crystal defects and to define the likely mechanical deformation systems of this material, in particular for crystals with a defect density too high for x-ray methods. Pure edge and pure screw dislocations with Burgers vector $\underline{b}$ = [010] were suggested to be the most prominent emergent dislocations.

A readily introduced twin plane was confirmed to be (101) and a preliminary study was made of twin generation under extensive strain to complement previous compressive strain studies. [28] Micro indentation and etching studies [29] proved that dislocation slip makes a major contribution to the plastic deformation of HMX. For crystals with a high defect density, etching is the preferred method of study; however, etching methods are restricted to the examination of defects formed close to or intersecting the crystal surface. They do not provide information on dislocations or other important imperfections contained within the bulk. Provided crystals of high perfection can be grown, the technique of X-ray diffraction topography can reveal the general growth induced defect structure in the bulk crystal. This allows assessment of the variations in internal perfection with growth conditions. In turn, it allows the formulation of conditions for the general improvement of the perfection of

product crystals and the better definition of the nature and behaviour of mechanically induced defects in the bulk crystal.

2 Experimental

2.1 Crystal growth: HMX powder of standard military grade (purity 99.5%), obtained from PERME, Waltham Abbey, was purified by multiple recrystallisation from distilled acetone (BDH Analar grade). Approximately 10 g of purified HMX was dissolved in 500 ml of acetone with constant stirring at a temperature just below the boiling point of the solvent. The solution was then allowed to cool slowly to room temperature before it was filtered into crystallizing dishes. A further 25 ml of solvent was added to each dish at the same temperature to ensure that the solution was slightly under saturated. The crystallizing dishes were covered and placed in the dark to allow spontaneously nucleated growth by solvent evaporation at a temperature of 293 K.

2.2 Specimen preparation: Only two small crystals were topographed in full. Otherwise all samples were prepared for transmission X-ray topography by cleaving crystals parallel to the {011} planes, polishing them on an acetone soaked cloth and washing carefully in a dish of the same solvent to remove surface damage. Alternatively, an entire crystal was thinned by polishing on an acetone soaked cloth.

2.3 X-ray topography:

Conventional X-ray Lang topographs, in which the crystal is scanned by a collimated x-ray beam, were recorded with an in-house constructed Lang Camera. Images were collected on Agfa Structurix D4 film using a monochromatic beam; Copper $K_{\alpha 1}$ (λ = 0.1541 nm) radiation.

The linear absorption coefficient, μ, of HMX for this wavelength (Cu $K_{\alpha 1}$) is 1.62 x 10^3 m^{-1}. For typical slice thicknesses between 0.75 mm and 1.25 mm, the important product μt has a value in the range 1.2 – 2.0. These absorption conditions correspond to the observation of essentially only direct images. The exposure times for recording the crystal images by this technique are lengthy and of the order of 12-24 hours.

Synchrotron X-ray topographs were collected at the STFC Daresbury Laboratory, on station 7.6 in projection mode. The images were recorded on Agfa Structurix D4 and D2 film, with a selected wavelength of λ = 0.154 nm for the recording of single topographs. The diameter of the synchrotron beam (~1cm) and its increased intensity allows the collection of a single topograph in the much reduced time of 30 – 300 seconds. An additional feature of the use of the full polychromatic beam is that, by using the Laue geometry, several images corresponding to different Bragg reflections can be collected in one exposure. As will be seen below this facility can be invaluable in the characterisation of

defects in the material from the variations in contrast of the images of the defects in different Bragg reflections.

3 Results and Discussion

3.1 Crystal morphology.

Growth by the described method yielded mainly small crystals of β-HMX less than 0.5 cm^3 in size, although larger crystals were also obtained. The dimensions and morphological appearance of the crystals selected for this study are summarized in Table 1, along with a diagram of the theoretical Bravais Friedel Donnay Harker (BFDH) morphology for HMX (Figure 1). Figure 2 shows typical examples of as grown crystals of HMX exhibiting the range of habits grown in this study. Prismatic crystals with well defined {010} forms grew in equant (P1) and elongated (P2) shapes. The tabular (T) forms showed dominant {011} faces. Crystals (D) were distorted tabular and were visually highly strained.

Occasionally small crystals closely similar to the calculated morphology were formed. Otherwise, the majority of crystals were elongated parallel to <100> and had a plate-like habit dominated by well-developed {011} faces with less important {110}, {010} and $\{10\bar{1}\}$ forms. In a small number of crystals, the

{10$\bar{1}$} faces were very small or absent, giving them a more prismatic shape. Twinning on {101} planes was prevalent in the smaller crystals, but occurred much less frequently for the larger crystals which grow under different supersaturation conditions. Many of the crystals exhibited 'hopper' growth on the lower faces due to faster growth at the edges rather than the face in contact with the bottom of the crystallizing dish.

Such variations in morphology are a regular feature when crystals are prepared using this simple method of growth. They result from the inability to accurately define or control the supersaturation in the growing system. The dominant morphology in this case, which differs from that predicted by theoretical calculations (Figure 1) [30-32], is defined by this method of growth.

Growth by self-nucleation, as used here, requires that the supersaturation of the crystallizing solution increases to a value in excess of that required to initiate nucleation. Once the nuclei are formed the supersaturation drops to lower values and growth continues. The consequent removal of solute, results in a gradual decrease and potential variation in supersaturation and hence a variation in the mechanisms and the rates of growth of the crystal faces. Coupled with the usual fact that the nucleating and growing solutions are not stirred (to discourage multi-nucleation), it is not surprising that wide variations in crystal habit occur. Despite this variation the predicted forms are usually always present in all self-

nucleated crystals as can be seen in the examples shown in Figure 2 and defined in Table 1. Thus they all show the characteristic defect structures of the various growth sectors.

The opinion of the authors, based on the comparison of the results of this method with better defined growth techniques [33-36]is that the prismatic crystals (Figure 2, P1) the morphology of which is closest to the theoretical morphological prediction, are representative of growth at lower supersaturation and will yield the most perfect crystals. This proposal is consistent with the relatively small size and low occurrence of specimens of this morphology. The increasing extension in the <100> direction (P2) and eventual dominance of the {011} forms (T and D) results from growth at successively increasing supersaturations. Such variations result from the onset of growth mechanisms that encourage the generation of gross imperfections in the crystal [33-36].

The solution to this variation is of course to grow crystals by seeded growth at constant lower supersaturation and under well-stirred conditions as was done in our previous studies of the growth of much larger crystals of TNT, PETN and RDX [15-17]. At the time that the present work was carried out it this did not prove to be satisfactory. Even delicate modes of supporting the small seed crystals caused sufficient damage to induce twins into the seed at the supporting point and to yield multiple rather than single crystal growth. There is of course no reason why continued work in this area should not be successful.

As grown, most crystals were too thick to allow the resolution of individual defects using transmission X-ray topography, therefore their thickness had to be reduced prior to examination. Attempts to slice the crystals using a solvent saw were unsuccessful as the rate of dissolution perpendicular to the slice plane was much faster than the cutting rate of the saw. This resulted in slices that were heavily pitted and holed and which cracked upon subsequent handling. Ultimately, it was found necessary to thin the larger ad thicker samples as described in the experimental section.

3.2 Crystal Perfection

3.2.1 X-ray topography

The dominance of the {010} and {011} forms (Figure 1) means that the distribution of growth defects is best viewed normal to these faces or from slices cut or cleaved parallel to these planes. Potential x-ray reflections were calculated using the unit cell of Cady [20] and the structure factors given by Eiland and Pepinsky [19]. Stereographic projections showing the important x-ray reflections for the two slice orientations, (010) and (011) are illustrated in Figures 3a and 3b. It can be seen from the stereogram shown in Figure 3a that numerous potentially useful x-ray reflections are accessible from the (010) slice plane. The location of many low index planes on the edge of the circle provides a large selection of high structure factor x-ray reflections making this

orientation particularly suitable for the characterisation of defects. Regrettably, only a few small, spontaneously nucleated crystals exhibited this sort of habit from which (010) slices could be obtained easily. In contrast those with dominant {011} forms had small or missing {010} faces. The stereographic projection of the {011} slice plane, illustrated in Figure 3b, is consistent with the lack of symmetry expected for this orientation and contains no low order symmetric reflections at all. Despite this handicap, with careful control of the diffraction geometry, the highly asymmetric $(02\bar{2})$ reflection was found to afford an acceptable view of the defect configuration of crystals sliced on (011) planes and was used almost exclusively. The resulting asymmetry of the experimental set-up (Figure 3c), leads to beam compression and hence distortion of the diffracted image compared with that expected for an orthogonal projection.

3.2.2 Radiation damage.

A potential problem with the use of the x-ray topographic techniques is that of the effects of radiation damage to the specimens and its influence on the interpretation of the results. The use of monochromatic laboratory sources presents few problems for most organic materials; including energetic materials. As we shall see below, for the most part these materials are sufficiently "radiation hard" not to show radiation damage even in the long exposure

conditions required. The more sensitive energetic materials must however be handled with care when examined with the higher powered synchrotron beam. Before proceeding to review the results of the studies on HMX crystals, it is appropriate to demonstrate the degree of radiation stability of this material.

Figure 4 shows a series of images reproduced from successive Laue topographs taken as a function of time exposure of a full (011) crystal to the full synchrotron beam. The thickness of the crystal does not allow the detailed reproduction of the defect structure of the specimen. The first image Figure 4a from a 7 minute exposure, when enlarged, shows images of dislocations (D) in the thinner, more perfect, upper and lower sectors of the crystal. Otherwise the image is dominated by the strained areas associated with superposed growth sectors (the block structures) and their boundaries. This observation defines well the part played by internal lattice strain from both growth sector boundaries and potentially, solvent inclusions on the radiation hardness of the material.

A total exposure of 10 minutes (Figure 4b) shows well that a degree of radiation damage has initiated by the general darkening and blurring of the image particularly in the region of the more highly strained growth sector boundaries. The dislocation images in the upper and lower sectors also have lost their clarity.

Progressing to longer exposures (14 minutes total Figure 4c) leads to a complete loss in clarity in the dislocation images and a total blurring of the overall image.

From this examination we see that for satisfactory recording of the defect structure exposures for either Laue or Bragg reflections should be restricted to exposures of no more than 7 – 8 minutes total and ideally as much lower than this as is required for the adequate production of a satisfactory image.

During the course of these exposures the initially transparent crystal turned an increasingly deeper yellow colour.

3.2.3 Prismatic Crystals

The prismatic crystals obtained during this study were, in general, small in size and few (Table 1). Thinning of the crystals proved difficult due to their shape and size. Lang topographs were taken of one full crystal in an attempt to form a link with our previous etching studies of the (010) faces of this type of crystal. Unfortunately no detailed characterization can be made of the results but some tentative observations can be made concerning the general defect structure

Figure 5a shows the (002) reflection Lang topographic image of a complete equant prismatic crystal (HMX 1), (Figure 2, P1). Arrays of bundles of growth dislocations emanate from the nucleation point and from the growth sector

boundaries between the upward growing (010) sector and the lateral faces. The dislocations travel to the lateral bounding facets. The overall dark contrast arises from the superposition of the images of dislocations occupying all lateral growth sectors in the depth of the crystal. The lighter contrast at the centre is the upward growing (010)sector indicated on Figure 5c. Since the nucleation point of this crystal will be immediately below the (010) surface there will be no superposition of defects in other sectors below this point. There are no other major defects than the dislocation bundles visible in this specimen. Figure 5b shows the (101) reflection Lang topograph. As with the previous figure, there are dislocation bundles emanating from the central portion of the crystal, however, some of the dislocation bundles visible in figure 5a are out of contrast in this image, showing that even with self-nucleated crystals, it is possible to generate initial defect contrast data.

An elongated prismatic crystal (HMX 8), (Figure 2, P2), was also examined using synchrotron Laue and Lang topography. This crystal was more defective than the type P(1) crystal in that distinct solvent inclusions dominate the topographic image. This change is indicative that between P(1) and P(2) other growth mechanisms more prone to solvent inclusion may have come into play to cause this change. The results are more appropriately discussed below in the section on Twinning (Figure 9) in which several topographs of this crystal are depicted

3.2.4 Tabular Crystals.

The tabular crystals were of a much greater size than the prismatic crystals and could be thinned to reveal greater detail of the development of the defect structure in the bulk crystal.

A clearer indication of the general growth characteristics can be seen from the image in Figure 6 the lower part of which is well contrasted. This is a $(02\bar{2})$ Lang topograph of a complete crystal (Table 1, HMX 3) elongated along the <100> direction. Thinning the slice has reduced the overlapping of defect images and revealed the general growth history of the crystal in the plane of the image. Below the upward growing $(01\bar{1})$ growth sector lies the nucleation point (N) from which extends growth sector boundaries (B) to the edges of the slice. These are heavily contrasted as a consequence of the strain built up between the differentially growing adjacent sectors and are an inevitable defect in any crystal. Also visible in the image are growth dislocations (D). These emanate from the central core and propagate within the growth sectors to the lateral bounding surfaces. The small defects (area P) in the lower right sector of the image are dislocations propagating in the near vertical direction to an upper facing surface. Also a regular feature are bands of varying contrast (C) parallel to the bounding faces that reflect variations in lattice strain arising from fluctuations in growth rate during the growth of the crystal.

Despite the appearance of the darker areas across the image that represent volumes of gross lattice strain potentially arising from inclusion of solvent, the crystal is in general of high perfection.

The complexity of the relationship between the various underlying sectors in this crystal can be judged from the schematic shown in Figure 6(c). A better representation of the detailed defect structure can be gained from the examination of topographs of adjacent slices in the depth of the crystal.

Figure 7 shows the result of such an examination. Figure 7a (HMX 4) and b (HMX 5) are schematic diagrams of the crystal sectioned, their shapes and crystallographic orientations. To demonstrate the relationships between the use of the Laboratory and Synchrotron techniques we compare Lang and synchrotron Bragg $(02\bar{2})$ topographs for equivalent samples.

Section (a) 2 is the lower (first crystallised) section of crystal HMX 4 (Figure 7a). At the centre is the nucleation point (N) of the crystal from which the morphology develops. This is always the most defective part of the growing crystal where it develops from a disordered nucleus to an ordered matrix. From this radiates the growth sector boundaries (B); the principal of which are the four black lines which emanate from the region of the nucleus. These surround the upper facing sector. Others can also be discerned facing towards the principal bounding faces: the lateral growth sectors. From the nucleation point many dislocations (Fine lines) emanate and travel to the growing faces. Their

number and character (edge, screw, or mixed) determine the growth rate of the crystal and hence its morphology. It is not possible to characterize fully the dislocations from this one image but dislocations that propagate normal to the crystal faces are likely to be of edge or screw character. Angled dislocations, by far the most present, will be of mixed edge/screw character. Other dislocation configurations can be found for example, the V shaped configurations in the right hand sector. These can be generated at inclusions, at points in the growth sector boundaries or other major defects in the crystal. Their V shape reflects their (structural) "positive and negative" character; one of each character having to be formed for balance in the perfect lattice. Again, present is Growth Banding, lines of varying contrast parallel to the crystal faces which can be seen in all the lateral sectors. Of particular interest is the dark area (X) at the top centre edge of the image. This is an area of mechanical damage consisting of overlapping bundles of dislocation loops punched into the crystal during the cleaving of the specimen from the original crystal. This testifies well to the easy introduction of dislocation slip as a major contribution to the mechanical deformation properties of HMX.

In contrast image Section (a) 1 looks more promising and appears to be much more perfect. It contains predominantly the upper facing (011) growth sector; reflected by the incomplete hexagon of darker contrast of the growth sector boundaries surrounding the central area of the image. The second longer side

has been eroded in the preparation of the specimen. Several points should be noted:

1. Along the lower edge of the crystal can be discerned a faint linear pattern. This is the eroded image of the missing lower boundary of the upper growth sector.

2. The end growth sectors are much more perfect than in the lower slice but some dislocation images are apparent in the left hand sector.

3. There are many dislocation images in the narrow (010) sector at the top side of the image; all of these are dislocations lie at high angles to the bounding surface.

4. The main (011) sector shows a variable contrast consistent with a variation of elastic strain in the sample. Of more importance however is the observation of a number of short parallel line images at a high angle to the surface. These are potentially images of dislocations crossing the sample from below and which would emerge on the upper (011) face. This speculation will be verified below by examination of the synchrotron radiation topographs of the same specimens.

Section (b) 3 is the equivalent slice to section (a) 1. Although it shows only half of the crystal, it is much less eroded at the upper edge and the defect structure of the (010) sector is well defined. An enlarged image shows dislocation images of three types; the majority at angles of approximately + and - 30° to the surface and a few normal to the surface. The former are of mixed character and the

latter of either edge or screw character. At C are dislocations propagating upwards in the slice at a high angle.

Overall, we have a situation where the greatest density of growth dislocation, are propagating from the nucleation point in and to the growing extreme of those sectors having a growth vector on the <100> directions. In the lateral directions the sectors contain many fewer dislocations. It is perhaps not surprising that the general morphological development is an elongation in the <100> direction.

3.2.5 Synchrotron Radiation Topographs

The following images in Figure 7 are Synchrotron Bragg reflection topographs of the same crystal as used for the foregoing Lang topographs. They all show the same basic defect structure but the synchrotron topographs show some additional detail arising from the slightly different x-radiation wavelength used for the exposures.

In Synchrotron Section (a)1 the contrast of the image has changed from that in Section Lang a(1) The more precise short dark lines in the upper sector can be more confidently accepted as dislocation alignments. Also, the narrow band of the upper sector has become clearer and the dislocations here are more obvious. They can now be seen to have the same alignment as in the clearer equivalent sector in Lang (b) 3 and Synchrotron (b) 3

The change in contrast has also "cleaned up" the bundle of mechanically induced dislocations in the upper sector of Section (a) 2 where they now appear as separated images. There are other subtle variations in the general picture of gross imperfections such as sector boundaries and inclusions.

From this comparison it be seen that the two topographic techniques have the complementary power to yield an immense amount of information on the growth defect structure of crystals and its relationship to growth conditions.

In the case of HMX we have a situation where the greatest density of growth dislocations are propagating from the nucleation point in and to the growing extreme of those sectors having a growth vector on the <100> directions. In the lateral directions the sectors contain many fewer dislocations and appear to be more perfect. It is perhaps not surprising that the general morphological development is an elongation in this direction. The crystals show a high degree of inclusions, growth banding and strain across the growth sector boundaries particularly in those sectors propagating in the faster growing <100> directions. This implies that under the conditions that yield tabular crystals directions faces with a growth vector in the <100> propagate not only by dislocation mechanisms but by a gradually increasing contribution from two-dimensional or rough growth mechanisms that are known to lead to the formation of solvent inclusion. [37] Such a conclusion is consistent with the observed significant departure from the theoretically predicted Donnay-Harker morphology form to which the prismatic crystals approximate. Recent studies, both practical and

theoretical support this conclusion both generally and more particularly in the case of HMX. [38,39]

3.3 Defect characterisation

3.3.1 Dislocations.

The description of the preceding experiments has been directed solely towards the analysis of the growth behavior and crystal quality of HMX as a first step towards the preparation of higher quality crystals. An eventual aim is to advance to the characterization of individual defects and their properties as has been carried out for other energetic materials. X-ray topography can also play a significant part in this aim.

As indicated however, crystals of the present major orientation present too few opportunities to access Bragg reflections of a significantly high structure factor to carry out such an analysis. The weaker structure factor reflections would require exorbitantly long exposure times to acquire suitable images by Lang topography. In fact only the g.$(0\bar{2}2)$ reflection is satisfactory within a reasonable time scale. The prismatic crystals with their larger (010) face would be more suitable but the preparation of suitably sized specimens has still to be achieved. The potential of such crystals is shown by the additional images presented in Figure 5 which shows a variation of dislocation contrast with g vector for the prismatic crystal. We would not proceed to suggest a

characterization in the complicated case of superimposed images but with a thinner slice of a more perfect crystal this would be possible. An alternative way forward is to use the increased power of the synchrotron and The Laue technique by which several Bragg reflections can be accessed at one short time. Figure 8 shows a typical Laue topograph of a slice of a tabular crystal (HMX ?) that has been placed normal to the synchrotron beam and exposed for 3 minutes. Nine potentially satisfactory images are obtained which immediately or with adjustments in exposure time could be usefully used for characterization purposes. The three sample images were extracted from this Laue and can be seen to have all the basic defect features shown in previous topographs. Each can be assigned a *g* vector and any variations in defect contrast defined. Unfortunately, in this case, closer examination of each image reveals no such difference. The dislocations obvious in the upper sector are present in all three images. The best that can be said are that they are of mixed character, as is usually the case for such growth dislocations.

The above demonstrates however the potential of the available topographic techniques to yield more detail of the character and behavior of dislocations. In a more perfect crystal, prior mechanical deformation by indentation or extension could lead to the introduction of a characteristic mechanically induced dislocation structures and hence their characterization.

3.3.2 Twinning

A particular characteristic of β-HMX is the ease with which it undergoes mechanical twinning when subjected to compressive or extensive stress. Mechanical twinning during growth was rarely observed. That such events are rare during crystal growth is perhaps understandable from previous microscope observations of the mechanical twin formation and behavior in HMX.

The initial observations of mechanically induced twins in HMX [28,29] were made following the compression or extension of an otherwise twin-free crystal. On releasing the stress the twin vanished; the crystal returning to its former transparency. This procedure could be repeated several times and to successively higher stresses before the twin remained permanently fixed in the crystal. Under the relatively stress free conditions of growth such a deformation is unlikely and more particularly, is even less likely to be permanent. Only a few cases should occur and luckily we were able to locate one.

Figure 9a shows the Synchrotron Laue of a mechanically twinned crystal. Twinning is immediately defined by the separation of the images of the twin band (T) from those of the parent image. Matching the Laue pattern of the twin images with that of the parent would give us the relative crystallographic orientations of the twin and the host lattice as was used in our similar observation of 180 degree twinning in TNT. [15] In the present case however a more direct approach can be made by studying the variation in diffraction contrast of the images as a function of the g vector of the radiation as signaled

above. Figure 9b, c and d shows three Lang topographic images of a P(2) prismatic crystal placed with its (010) face normal to the incident beam; each taken using a specific x-radiation *g* vector. The absence of the twin band in the *g*,002 and *g*,200 reflections and its presence in the *g*,101 is definitive evidence for the twin plane being $(01\bar{1})$. Variations in the twin direction mirror the low index crystallographic directions of the crystal structure. This assignment is in accord with the previous optical studies. [27]

4 Conclusions

This study advances the fundamental knowledge of the energetic material HMX in several respects. It opens the way to the better understanding of its energetic and thermal properties with respect to their potential association with the bulk defect structure. The association of that structure with growth conditions is defined and shown to be in satisfactory agreement with existing general knowledge of the influence of supersaturation on the morphology of crystals and their perfection. It accords with the recent theoretical calculations of the potential influence of growth conditions, particularly supersaturation, on the mechanisms of growth and hence perfection of HMX crystals. In turn the success of the x-ray topographic technique, in all its manifestations opens the way for the more detailed study of the growth and mechanically induced defect structure than presently possible. With the availability of larger sized crystals of the prismatic form, which should be possible based on the present work, the

relative contributions of dislocation motion and twinning to the mechanical deformation of HMX can be established. The successful production and deformation of more perfect crystals should lead to the full characterisation of both growth and mechanically induced dislocations and their properties and the structural and/or defect source of the initiation and stability of the mechanical twinning in this material as has been done previously for other energetic materials.

Acknowledgements

This work was made possible principally by the financial support of the European Office, US Navy and for which JNS and HGG express their grateful thanks. The UK SERC is thanked for the provision of additional facilities provided by their general financial support of the Strathclyde laboratories. The synchrotron topographic studies were carried out on Station 7.6 the UK Synchrotron Radiation Facility provided by the UK SERC at Daresbury, UK. The authors thank the Director and his Staff for their kind help in this respect.

References

1) High Resolution X-ray Diffractometry and Topography, D. Keith Bowen and Brian K. Tanner, Taylor and Francis, 2005
2) B.D. Chapman, A Checco, R. Pindak, T. Siegrist & C. Kloc, Dislocations and grain boundaries in semiconducting rubrene single-crystals, J. Crystal Growth, (2006) 290, 479-484

3) M. Koishi, N. Oyha, Y. Mukobayashi, H. Koizumi, K. Kojima and M. Tachibana, Observation of clear images of dislocations in protein crystals by synchrotron monochromatic beam x-ray topography, Crystal growth and design (2007) 7 2182-2186
4) P.J. Halfpenny, J.N. Sherwood and G.S. Simpson, The Growth and Perfection of Organic Non-linear Optical Materials, in Non-linear Optical Materials, Proceedings of the 125th Course of the International School of Physics "Enrico Fermi". (Editors V. Digiorgio and C. Flytzanis: IOS Press, Amsterdam,1995.
5) P.J. Halfpenny, K.J. Roberts & J.N. Sherwood, Dislocations In Energetic Materials I. The Crystal Growth And Perfection Of Pentaerythritol Tetranitrate (PETN), Journal of Crystal Growth, 67, (1984) 202-212
6) P.J. Halfpenny, K.J. Roberts & J.N. Sherwood, Dislocations In Energetic Materials IV. The Crystal Growth And Perfection Of Cyclotrimethylene Trinitramine (RDX), Journal of Crystal Growth, 69, (1984) 73-81
7) R. W. Armstrong and Wayne L. Elban; Materials Science and Technology Aspects of Energetic (Explosive) Materials, Materials Science and Technology, 22, 4, (2006), 381-395
8) J.E. Field, Hot spot ignition mechanisms for explosives, Acc. Chem. Res. (1992), 25, 489-496
9) S. Sorber, C. Stennett and M. Goldsmith, Developments in a small scale test of violence, AIP Conf. Proc. 1426, (2012), 563-566.
10) X.H. Duan, W.P. Li, C.H. Pei and X.Q. Zhou, Molecular dynamics simulations of void defects in the energetic material HMX, Journal of Molecular modelling, (2013) 19, 3893-3899
11) T. Zhou, J. Lou, Y. Zhang, H. Song and F. Huang, Hot spot formation and chemical reaction initiation in shocked HMX crystals with nanovoids: a large scale reactive molecular dynamics study, PCCP, (2016), 18, 17627-17645
12) Daniel E. Hooks, Kyle J. Ramos, C. A. Bolme & Marc C. Cawkwell; Elasticity Of Crystalline Molecular Explosives, Propellants, Explosives and Pyrotechnics, 40, (2015) 333-350
13) R.A. Pethrick, J.N. Sherwood and C.S. Yoon, Ultrasonic Studies of benzophenone single crystals I. Influence of defect structure, Philosophical Magazine A, (1992), 65, 1021-1032
14) R.A. Pethrick, J.N. Sherwood and C.S. Yoon, Ultrasonic Studies of benzophenone single crystals II. Elastic constant measurements on a perfect single crystal, Philosophical Magazine A, (1992), 65, 1033-1047

15) H.G. Gallagher, R.M. Vrcelj & J.N. Sherwood, The Crystal Growth And Perfection Of 2,4,6-Trinitrotoluene, Journal of Crystal Growth, 250 (2003) 486-498
16) Halfpenny PJ, Roberts KJ, Sherwood JN: Dislocations in energetic materials. II. Characterization of the growth-induced dislocation structure of pentaerythritol tetranitrate (PETN). J Appl Cryst 1984, 17:320–327.
17) Halfpenny PJ, Roberts KJ, Sherwood JN: Dislocations in energetic materials.4. The crystal-growth and perfection of cyclotrimethylene trinitramine (RDX). J Cryst Growth 1984, 69:73–81.
18) Halfpenny PJ, Roberts KJ, Sherwood JN: Dislocations in energetic materials - dislocation characterization and postgrowth motion in single-crystals of cyclotrimethylene trinitramine. Phil Mag A 1986, 53:531–542.
19) P.F. Eiland and R. Pepinsky, The crystal structure of cyclometylene tetranitramine, Z. Kristallogr. (1955) 106 273 - 298
20) H.H. Cady, A.C. Larson & D.T. Cromer, The Crystal Structure Of α-HMX and a Refinement Of The Structure Of β-HMX, Acta Cryst. (1963) 16 617-623
21) Choi CS, Boutin HP: A study of the crystal structure of β-cyclotetramethylene tetranitramine by neutron diffraction. Acta Cryst 1970, B26:1235–1240.
22) Zhurova EA, Zhurov VV, Pinkerton AA: Structure and Bonding in β-HMX Characterization of a Trans-Annular N · · · N Interaction. J Am Chem Soc 2007, 129:13887–13893
23) Deschamps JR, Frisch M, Parrish D: Thermal Expansion of HMX. J Chem. Cryst 2011, 41:966–970
24) Cobbledick RE, Small RWH: The crystal structure of the delta-form of 1,3,5,7-tetranitro-1,3,5,7-tetraazacyclooctane (δ-HMX). Acta Cryst 1974, B30:1918–1922.
25) Korsunsky BL, Aldoshin SM, Vozchikova SA, Golovina NI, Chukanov NV, Shilov GV: A new crystalline HMX polymorph: ε-HMX. Russ J Phys Chem 2010, 29:934–941
26) P. Main, R.E. Cobbledick & R.W.H. Small, Structure Of the 4th Form Of 1,3,5,7 – tetranitro-1,3,5,7 tetraazacyclooctane (γ-HMX) $2C_4H_8N_8O_8.0.5H_2O$, Acta Cryst. (1985) C41 1351-1354
27) H.G. Gallagher, J.N. Sherwood & R.M. Vrcelj, Growth and Dislocation Studies Of β-HMX, Chemistry Central Journal, (2014) 8 75
28) S.J.P. Palmer and J.E. Field, The deformation and fracture of beta-HMX, Proc. R. Soc. Lond. A (1982) 383, 399-407

29) H.G. Gallagher, J.C. Miller, D.B. Sheen, J.N. Sherwood & R.M. Vrcelj, Mechanical Properties Of β-HMX, Chemistry Central Journal, (2015) 9 22
30) SHAPE. http://www.shapesoftware.com
31) J.D.H. Donnay & D. Harker, A New Law Of Crystal Morphology Extending The Law Of Bravais, American Mineralogy, (1937) 22, 446-467
32) E. Dowty, Crystal structure and crystal growth: I. The influence of internal structure on morphology, American Mineralogy, (1976) 61, 448-459
33) K.V.R. Prasad, R.I. Ristic, D.B. Sheen, J.N. Sherwood, Crystallization of paracetamol from solution in the presence and absence of impurity, Intl. J. Pharm. (2001) 215, 29-44
34) R.I. Ristic, S. Finnie, D.B. Sheen and J.N. Sherwood, Macro- and micromorphology of monoclinic paracetamol grown from pure aqueous solution, J. Phys. Chem. B (2001) 105 9057-9066
35) K. Srinivasan, J.N. Sherwood, Asymmetric growth of α-resorcinol crystals: Comparison of growth from the vapour phase and from aqueous solution, Cryst. Growth and Des. (2005) 5, 1359-1370
36) W. Hou, R. I Ristic, R. M. Vrcelj, D. B. Sheen and J. N. Sherwood, Crystal growth of the acentric organic non-linear optical material methyl-p-hydroxybenzoate (mhb): morphological variations in crystals grown by physical vapour transport. In Preparation
37) A.A. Chermov, Formation of crystals in solution, Contemp. Phys. (1989) 30, 251-276
38) H-M. Shim and K-K. Koo, Prediction of growth habit of β-Cyclotetramethylene-tetranitramine Crystals by the First Principles Models, Crystal Growth and Design, (2015), 15, 3983-3991
39) T. Yan, J-H. Wang, Y-C. Liu, J. Zhao, Y-M. Yuan and J-H. Guo, Growth and morphology of 1,3,5,7-tetranitro-1,3,5,7-tetraazacy-clooctane (HMX) crystal, Journal of Crystal Growth, (2015), 430, 7-13

Figure 1: Morphology of the predicted SHAPE HMX crystal
Figure 2: Morphological appearance of the as-grown crystals of HMX. Examples of prismatic crystals as equant (P1) and elongated (P2) shapes, tabular (T) forms and distorted (D). The scale bar shows the general size of the crystals used in this study.
Figure 3: Stereographic projections for (a) (010) normal and (b) (011) normal to the direction of viewing. (c) The expected distortion of the recorded image of the crystal.
Figure 4: Synchrotron radiation damage effects on the images during successive exposures of an HMX crystal (HMX ?) to the synchrotron beam for the (004) reflection (a) 7min (b) 10min (c) 14 min
Figure 5: Lang X-ray topographs of a full equant prismatic crystal as viewed with X-ray *g*-vectors. (a) *g, 002* (b) *g, 101* (c) shows the distribution of the growth sectors. The white circled notch on the images indicates a point of equivalence.
Figure 6: (a) $(02\bar{2})$ reflection Lang topograph of an $(01\bar{1})$ slice of a tabular crystal (b) schematic showing the complex nature of the growth sectors and their defect content and (c) the general crystal shape.
Figure 7: (a) Sections of crystals HMX 4 and (b) HMX 5. (c) Lang topographs of sections and (d) Synchrotron topographs of sections. The annotations follow the meanings given previously for Figure 5.
Figure 8: A typical Laue topograph and three extracted images. The respective g-vectors are 1) *g, 210*; 2) *g,* $\bar{1}2\bar{1}$ and 3) *g,* $\bar{2}10$.
Figure 9: (a) Laue topograph of an elongated prismatic crystal (HMX 8) showing the displacement of the twin images (e.g. T) relative to the images of the parent crystal. (b), (c) and (d) Lang topographs with, respectively, *g*-vectors *200*, *004* and *101*.

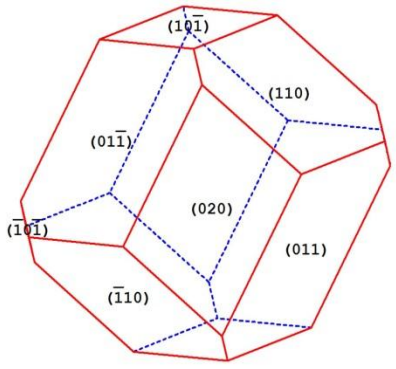

Figure 1

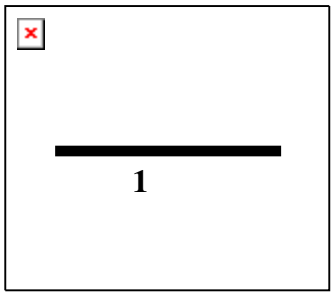

P(1)

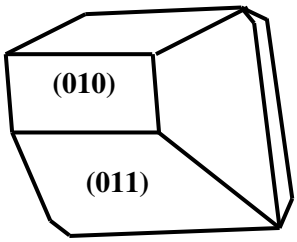

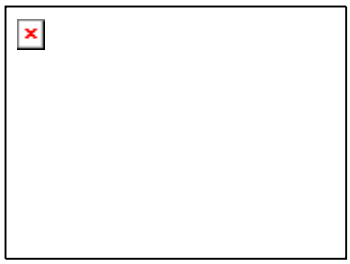

P(2)

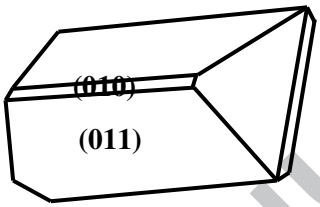

Fig

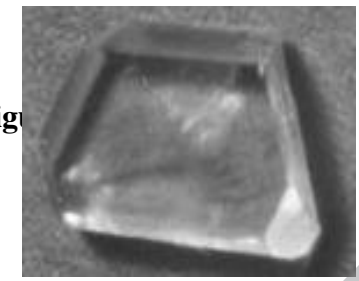

T

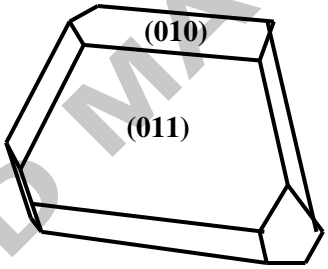

D

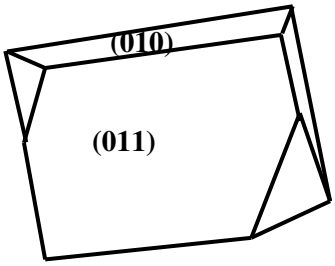

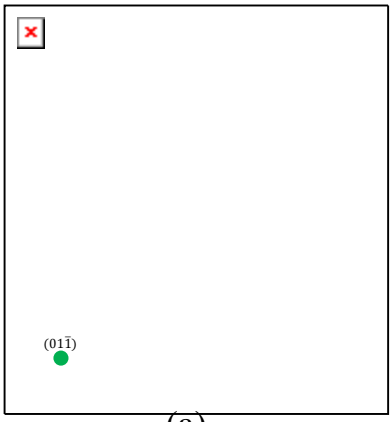

(a)

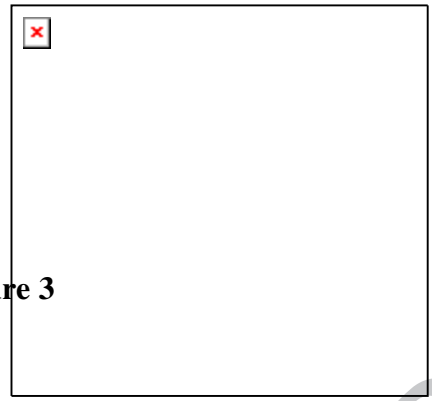

(b)

(c)

Figure 3

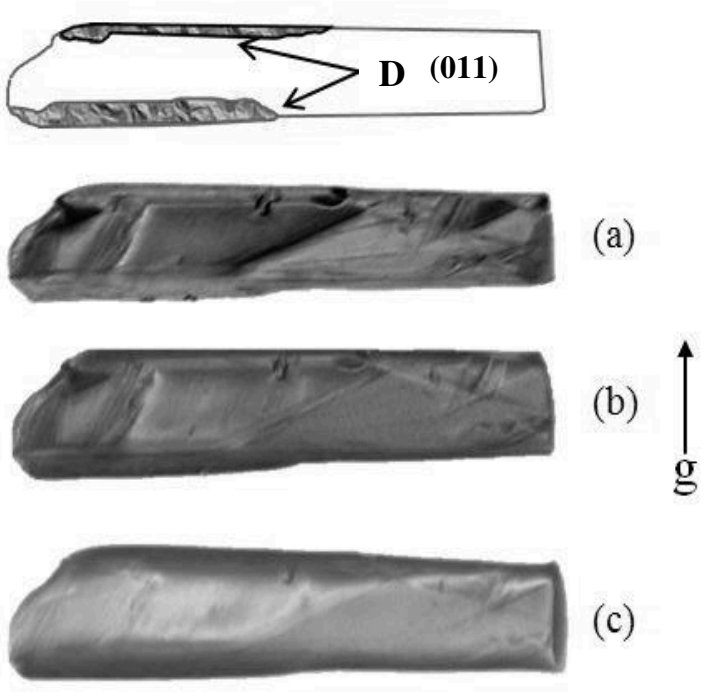

Figure 4

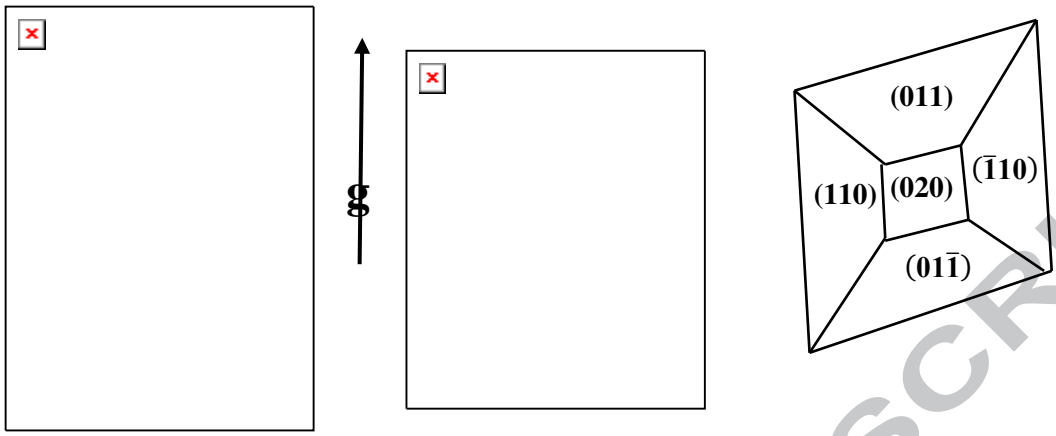

Figure 5

(a) (b) (c)

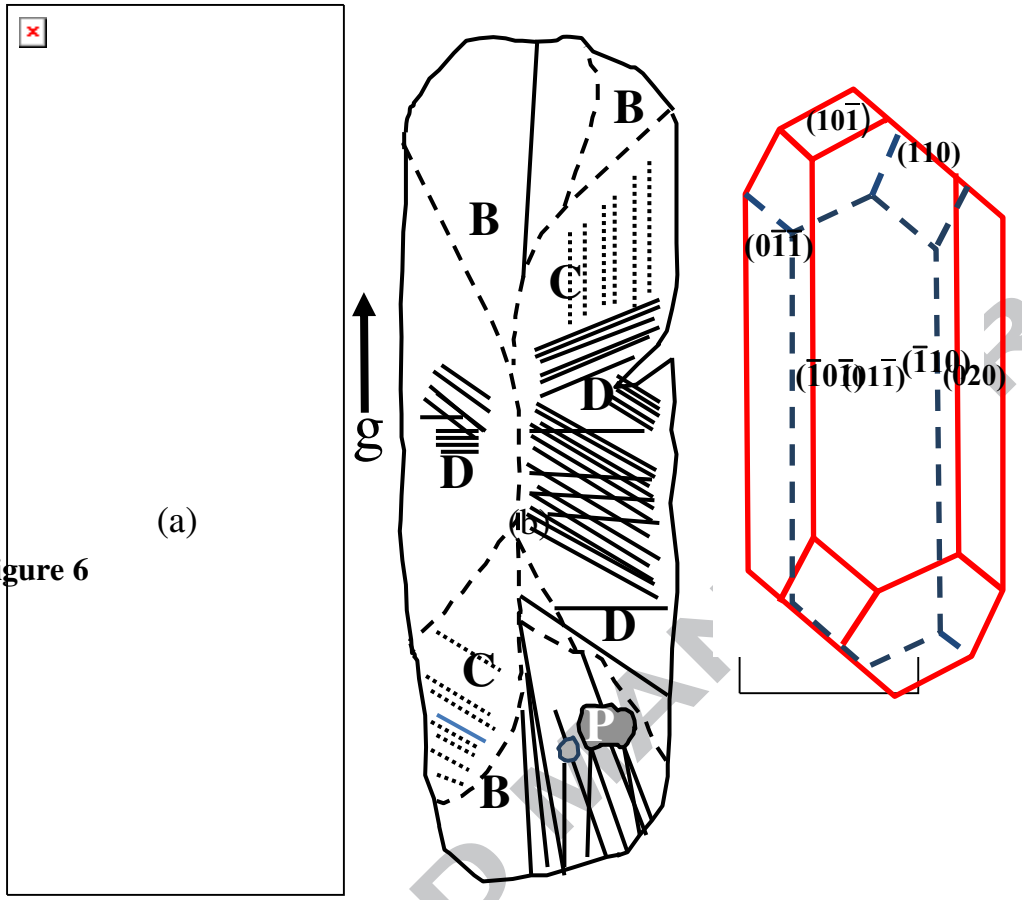

Figure 6

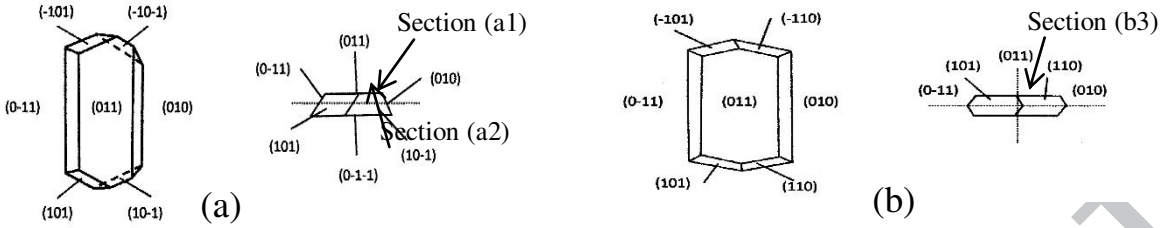

Lang topographs

Section (a) 1

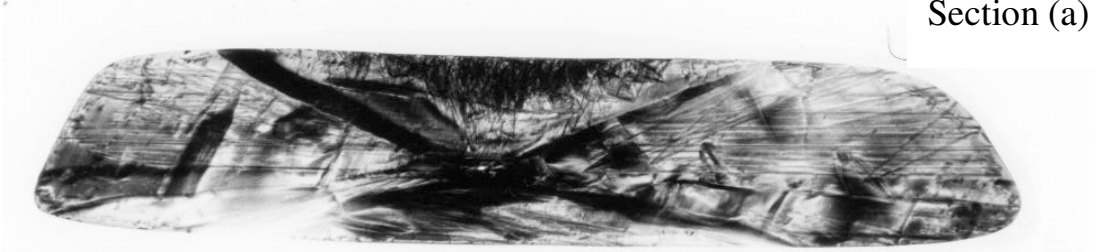

Section (a) 2

g

Section (b) 3

Synchrotron topographs

Section (a) 1

Section (a) 2

Figure 7

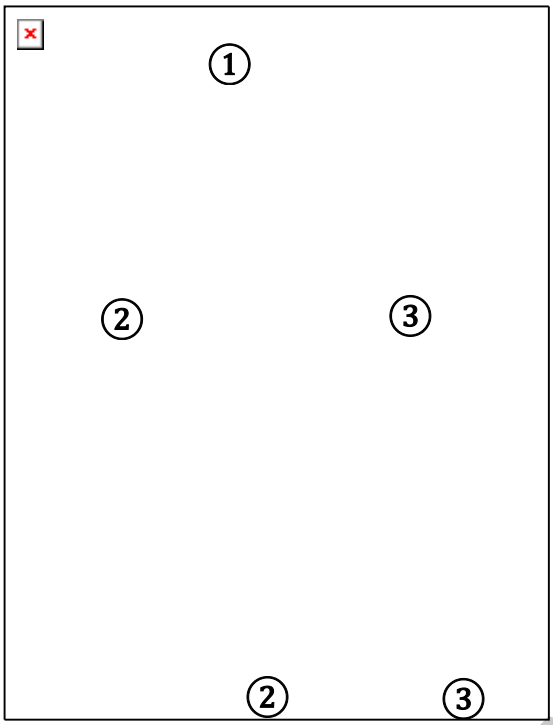

Figure 8

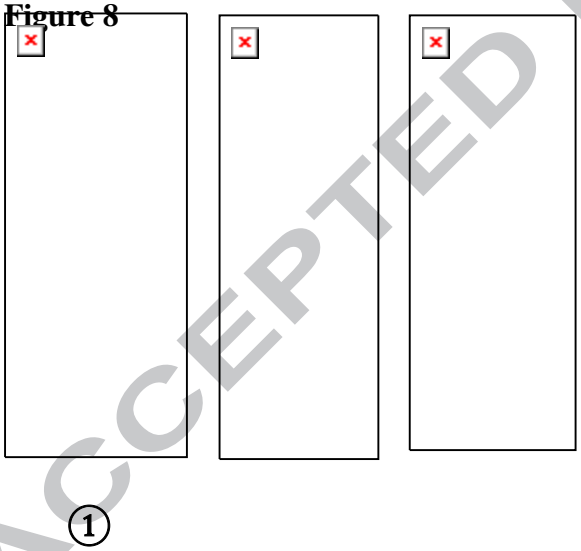

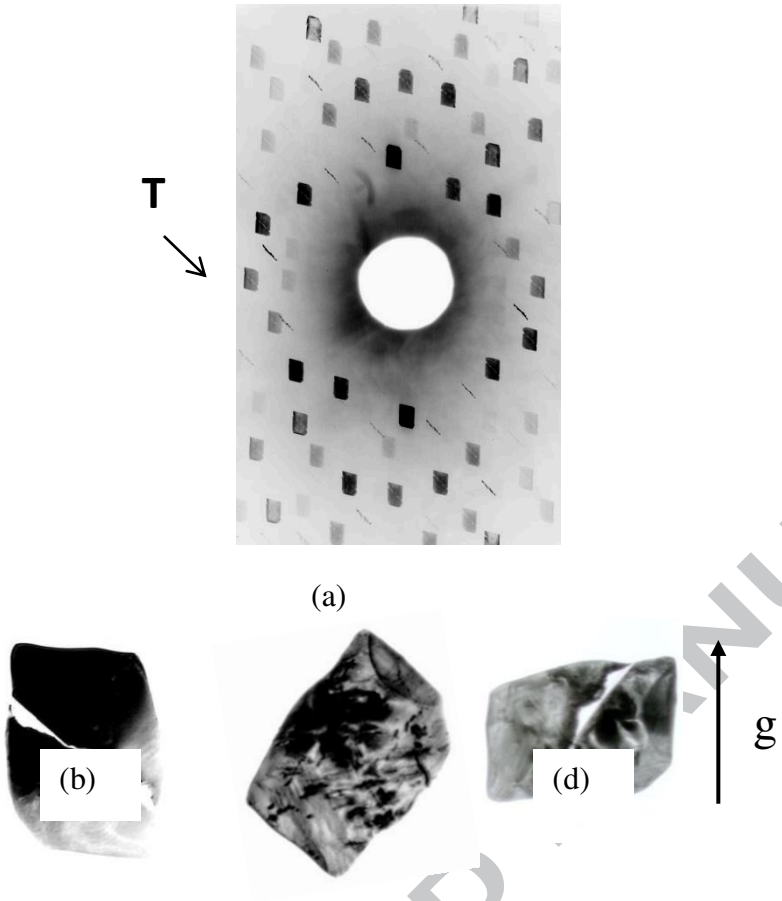

Table 1: Dimensions and morphological forms of the as grown and predicted SHAPE HMX crystals.

Table 1

Crystal Number	Habit	Dimensions (mm^3)	{011}	{01$\bar{1}$}	{010}	{110}	{$\bar{1}$01}	{$\bar{1}$10}	{101}
HMX 1	Prismatic	5 x 5 x 3	✓	✓	✓	✓	-	✓	**-**
HMX 2	Prismatic	7 x 5 x 3	✓	✓	✓	✓	-	✓	**-**
HMX 3	Plate-like	15 x 7 x 3	✓	✓	✓	✓	✓	✓	✓
HMX 4	Plate-like	16 x 4 x 2	✓	✓	✓	-	✓	-	✓
HMX 5	Plate-like	16 x 10 x 3	✓	✓	✓	✓	✓	✓	✓
HMX 6	Plate-like	12 x 7 x 2	✓	✓	✓	✓	✓	✓	✓
HMX 8	Prismatic	21 x 10 x 8	✓	✓	✓	✓	-	✓	**-**
Theoretical Donnay-Harker SHAPE prediction (equant prismatic) [30]. Shown schematically in Figure 1			✓	✓	✓	✓	✓	✓	✓

Differences in morphology of solution grown HMX crystals
The complexity of defect type and structure within HMX crystals
The effects of radiation damage on single crystals of HMX